Mathematical Biosciences and Engineering

MBE, 20(3): 5135–5158.
DOI: 10.3934/mbe.2023238
Received: 15 October 2022
Revised: 04 December 2022
Accepted: 18 December 2022
Published: 09 January 2023

http://www.aimspress.com/journal/MBE

Research article

Safety action over oscillations of a beam excited by moving load via a new active vibration controller

Hany Bauomy[1,2,*]

[1] Department of Mathematics, College of Arts and Science in Wadi Addawasir, Prince Sattam Bin Abdulaziz University, P.O. Box 54, Wadi Addawasir 11991, Saudi Arabia
[2] Department of Mathematics, Faculty of Science, Zagazig University, Zagazig 44519, Egypt

* **Correspondence:** Email: hany_samih@yahoo.com.

Abstract: This paper presents a mixed active controller (NNPDCVF) that combines cubic velocity feedback with a negative nonlinear proportional derivative to reduce the nonlinear vibrating behavior of a nonlinear dynamic beam system. Multiple time-scales method treatment is produced to get the mathematical solution of the equations for the dynamical modeling with NNPDCVF controller. This research focuses on two resonance cases which are the primary and 1/2 subharmonic resonances. Time histories of the primary system and the controller are shown to demonstrate the reaction with and without control. The time-history response, as well as the impacts of the parameters on the system and controller, are simulated numerically using the MATLAB program. Routh-Hurwitz criterion is used to examine the stability of the system under primary resonance. A numerical simulation, using the MATLAB program software, is obtained to show the time-history response, the effect of the parameters on the system and the controller. An investigation is done into how different significant effective coefficients affect the resonance's steady-state response. The results demonstrate that the main resonance response is occasionally impacted by the new active feedback control's ability to effectively attenuate amplitude. Choosing an appropriate control Gaining quantity can enhance the effectiveness of vibration control by avoiding the primary resonance zone and unstable multi-solutions. Optimum control parameter values are calculated. Validation curves are provided to show how closely the perturbation and numerical solutions are related.

Keywords: perturbation technique; beam; stability; resonance case; mixed controllers

1. Introduction

Unwanted vibrations have a detrimental impact on the functionality and, in certain severe circumstances, the structural integrity of machinery and other constructions. Establishing the conditions required to get rid of these undesirable operating states is essential in order to modify the modal properties of the applicable structural elements of the mechanical system. Basic structural components called beam structures are employed in both civil and mechanical structures. One of the main objectives in the structural design of beam constructions should be the capacity to minimize or lessen the degree of undesired vibrations. The dynamical properties of beam structures [1–3] are determined by their structures, geometrical parameters, and material properties. Beam structures frequently lack the required dynamic properties because they are typically made of homogeneous materials. In recent decades, there has been a lot of interest in the dynamic problems of structures subjected to moving loads [4–10]. The dynamics of multi-span bridges excited by a moving object with numerous degrees of freedom were studied by Marchesiello et al. [11]. Fryba [12] examined numerous straightforward moving-load issues in his monograph and offered analytical responses. Vibration control is a significant challenge, in addition to the dynamic modeling and analysis of civil and mechanical structures. Passive, semi-active, active, and hybrid vibration control methods have been developed [13–16].

Due to research showing that active control of structures is a more effective method than passive control [17,18], it has grown in popularity. For active structural control, there are numerous control algorithms based on control theory, such as PID control [13], optimal control [19], adaptive control [20,21], and intelligent control [22]. Due to the increasing speed of moving mass and structural flexibility, vibration control of beams subjected to a moving mass has recently received a lot of interest in both physics and engineering [23–26]. Since the analytical solution to the flexible structure model is commonly stated in modal space, independent modal space control is a key technique in the vibration control of flexible structures. The well-known phenomenon of spillover presents one of the major difficulties in the modal space control of flexible systems [27,28]. Positive position feedback (PPF) control is a simple and efficient control approach in practical applications [29,30] due to its fundamental property of being insensitive to spillover, or the capacity to regulate the target mode independently without affecting other uncontrolled modes.

Optimal control in modal space is the most widely used method for reducing vibration in a beam caused by a moving mass [31,32]. It is anticipated that the regulated state can be established using all of the measured or estimated data. But it's likely that not all sensors will be installed in order to capture the whole set of states [33]. Modeling and measurement errors are inevitable in real-world implementations. Therefore, to correct modeling errors brought on by modal truncation and measurement errors, a robust control mechanism is required. A powerful, resilient control method that can handle both outside disturbances and modeling uncertainty is sliding mode control (SMC) [34,35]. Qiu et al. [36] created a type of discrete-time sliding mode control approach to lessen the vibration of a flexible plate. Bauomy and EL-Sayed [37–41] developed several constructed control techniques that were used to control harmful vibrations caused by various nonlinear dynamical systems.

A novel magneto-electro-elastic (MEE) model of bi-directional (2D) functionally graded materials (FGMs) beams is developed for investigating the nonlinear dynamics [42]. The outcomes appear that the MEE materials significantly affect the asymmetric modes, which can further vary the mechanics of 2D FG beams. Furthermore, the three-directional (3D) functionally graded materials (FGMs) are

used to fabricate the slender beams to resist 3D loads and study the nonlinear mechanics to provide an insight reference for possible applications [43]. It is found that the three directional FG indexes can tune the mechanical performance of the beam, such as improving on the load-bearing capacity and enhancing in the flexibility of dynamic design, which is tremendously different from nonlinear behaviors of 2D and 1D FGMs beams. Besides, a novel model of bi-directional (2D) functionally graded materials (FGMs) nanobeams resting on the Pasternak foundation under the magneto-electro-elastic (MEE) fields based on the Timoshenko beam theory is presented to investigate the dynamic interaction behavior [44]. Formerly, the mathematical model of the non-prismatic Timoshenko beam considering shear and bending deformations is developed [45]. The numerical analyses of forced vibrations of the beam show that its points oscillate in different manners depending on their relative position along the beam. Therefore, a novel fractional order PDμ control of lattice grid beam with piezoelectric fiber composite face sheets is proposed [46]. Consequently, it is proved that the fractional order PDμ control can reduce the vibration amplitude of lattice grid beam more significantly and more rapidly, by comparing its numerical results with those of the integer order PD algorithm and uncontrolled results. Also, a recently-developed metaheuristic method called Crystal Structure Algorithm (CryStAl) is used to achieve optimized vibration control in structural engineering [47]. At last, the nonlinear free and forced vibration of functionally graded strain gradient Timoshenko microbeam are analytically investigated [48]. The analytical mode shapes are then closely verified via numerical simulations and the effect of different parameters on the fundamental natural frequency of the beam is studied.

The key goal of this research is to provide a new active controller strategy for removing high vibrations of the specified beams model via a suitable control technique.

The new active control includes increasing the nonlinear parameters such as negative cubic velocity feedback and a nonlinear negative proportional derivative controller in order to further eliminate the potentially harmful vibrations of the related framework. The system is made more stable by the researched controller, which comprises NNPD plus CVF as a new nonlinear control approach (NNPDCVF). The analytical result received by using multiple-time scales technique process near two resonances of primary and 1/2 subharmonic responses of a dynamical beam with moving load. The comprehensive mathematical solutions, frequency response equations (FREs), and stability analysis with NNPDCVF process are obtained using the perturbation method. Numerical solution and effect of all parameters on the vibrating system and the controlled system are plotted and reported. The MATLAB software is used to simulate the impact of various parameters and the controller on the system. The validations of the analysis's time history and frequency response curves (FRCs), as well as the numerical results, were satisfied by comparing them. Before and after providing the controller in the two measured resonance cases, the system is numerically and graphically examined. The simulation outcomes give that the new controller NNPDCVF method is found to be the most effective at eliminating high vibrations and making the system more stable. Finally, numerical results are obtained that show an outstanding agreement per the analytical results.

2. Governing equations and perturbation solution

As indicated in Figure 1, the dynamic beam structure is subjected to the dynamic load P, which transfers along the longitudinal direction of the beam with a velocity V within the novel active control method by a servomechanism. The beam's motion equation is given as follows [14]:

$$EIv'''' + m\ddot{v} + c\dot{v} = P\delta(x - Vt) + M_0\delta'(x - a) - M_0\delta'(x - L + a) \tag{2.1}$$

where the prime indicates the derivative with respect to x and the dot indicates the derivative with respect to t; E is the Young's modulus of the beam; I is the moment of inertia of the cross-section; $v(x,t)$ is the transverse displacement of the beam; m is the mass per unit length of the beam; c is the damping coefficient; δ is the Dirac delta function and δ' is the derivative; L is the span length of the beam; a is the distance between the servohinge and the end of the beam; In order to balance the bending deformation of the beam under a moving load, a servomechanism is installed below the middle of the beam span to generate a control torque M_0. The working principle is to adjust the control spring to attain the desired control effect. The control torque is designated as:

$$M_0 = lK\Delta = Kl[u(t) + l\,v'(a,t) - l\,v'(\mathrm{L} - a,t)] \tag{2.2}$$

where K remains the stiffness of the spring; l stands the arm length of servomechanism; $u(t)$ remains the spring displacement caused by servomechanism, and Δ is the displacement of the spring. When $u(t) = 0$, it is a passive control system.

The transverse displacement $v(\mathrm{x},t)$ can be expressed in terms of the expansion using the Galerkin method:

$$v(\mathrm{x},t) = \sum_{k=1}^{N} q_k(t)\,\phi_k(x) \tag{2.3}$$

where $q_k(t)$ is the generalized displacement; $\phi_k(x) = \sin(\mathrm{k}\,\pi\,\mathrm{x}/\,\mathrm{L})$ is the k-th mode shape; N is the number of the shape functions used in the approximation. Substituting Eq (2.3) into Eq (2.1), multiplying both sides of the resulting equation by $\phi_k(x)$ and integrating over the span of the beam, the j-th mode can be obtained as [14]:

$$\ddot{q}_k(t) + 2\zeta\omega_k\dot{q}_k(t) + \omega_k^2 q_k(t) = \frac{2P}{mL}\sin(k\omega t) - \frac{4k\pi M_0(t)}{mL^2}\cos(\mathrm{k}\,\pi\,\mathrm{a}/\,\mathrm{L})\sin(k\pi/2) \tag{2.4}$$

where $q_k(t) = (2/L)\int_0^L v(x,t)\,\phi_k(x)\,dx$ is the beam displacement of the k-th mode, ζ is the damping ratio, $\omega_k = [(k^4\pi^4/L^4)(EI/m)]^{1/2}$ is the natural angular frequency of the k-th mode, $\omega = \pi V/L$ is the natural angular frequency, and

$$M_0(t) = lK\Delta = Kl[u(t) + 2l\sum_{k=1,3,5,..}^{\infty}\frac{k\pi}{L}\cos\frac{k\pi a}{L}q_k(t)] \tag{2.5}$$

Only the fundamental mode is taken into account because the high order modes of motion barely affect bending displacement and the nonlinear features. The motion equation can therefore be found as

$$\ddot{q}(t) + \omega_0^2 q(t) + \mu\dot{q}(t) = f\sin(\omega t) + \alpha q^3(t) \tag{2.6}$$

The modified controlled system is

$$\ddot{q}(t) + \omega_0^2 q(t) + \varepsilon\mu\dot{q}(t) = \varepsilon f\sin(\omega t) + \varepsilon f\, q(t)\sin(\omega t) + \varepsilon\alpha q^3(t) + \varepsilon\beta q^2(t) + u(t) \tag{2.7}$$

where,

$$q(t) = (2/L)\int_0^L v(x,t)\phi_1(x)dx,\ \omega_0^2 = \omega_1^2 - 2\pi Kl\cos\frac{\pi a}{L}, \mu = 2\zeta\omega_1, f = 2P/(mL), \alpha = \pi^4 E^2/(L^4A^2),$$

$\beta = \pi^2 E/(L^2 A)$, A stands the cross-section area of the beam. $u(t)$ is the active control force which consists of mixed of negative nonlinear proportional derivative (NNPD) and cubic velocity feedback (CVF) controller which called (NNPDCVF) controller that is in the form

$$u(t) = -\varepsilon(p_1 q(t) + \mathrm{d}_1\dot{q}(t) + \alpha_1 q^3(t) + \alpha_2 q^2(t)\dot{q}(t) + \alpha_3 q(t)\dot{q}^2(t) + \mathrm{G}_1\dot{q}^3(t))$$

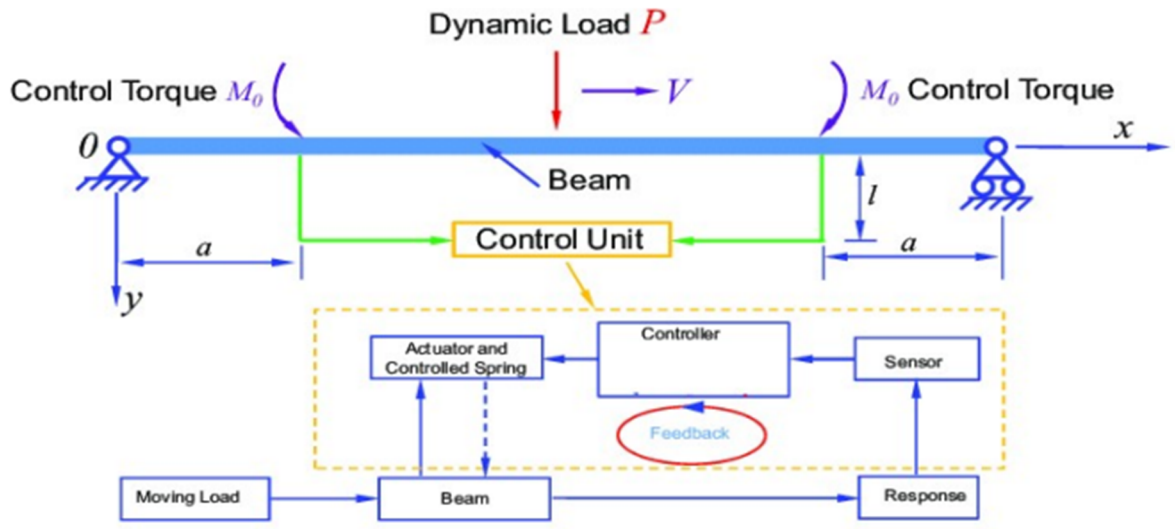

Figure 1. The simple controlled beam structure model.

3. NNPDCVF influences of various resonance cases of the framework

In this section, the new controller NNPDCVF method will be studied with different effective resonance cases that have acted on the vibrations of the system. The primary, internal, and subharmonic resonances of the new controller NNPDCVF are studied.

3.1. Primary resonance case $\omega \approx \omega_0$

To find the approximate solution of Eq (2.7), it is helpful to apply the method of multiple scales [49,50] as follows:

$$q(t,\varepsilon) = q_0\left(T_0, T_1\right) + \varepsilon q_1\left(T_0, T_1\right) + O(\varepsilon^2) \tag{3.1}$$

where ε is the perturbation parameter, $T_0 = t$, $T_1 = \varepsilon t$ are the two time scales.

The two time scales that can be used to express the time derivatives of Eq (2.7) are as follows:

$$\frac{d}{dt} = D_0 + \varepsilon D_1 \ , \ \frac{d^2}{dt^2} = D_0^2 + \varepsilon(2D_0D_1), \quad D_n = \frac{\partial}{\partial \mathrm{T}_n} \ (n = 0,1) \tag{3.2}$$

Assume, in the case of primary resonance,

$$\omega = \omega_0 + \varepsilon\sigma \tag{3.3}$$

where σ is detuning parameter. The following results are obtained by inserting Eqs (3.1)–(3.3) relevant to Eq (2.7), comparing coefficients of similar power of ε as

$O\left(\varepsilon^0\right)$:

$$\left(D_0^2 + \omega_0^2\right) q_0 = 0 \tag{3.4}$$

$O\left(\varepsilon^1\right)$:

$$\left(D_0^2 + \omega_0^2\right) q_1 = -2(D_1D_0)q_0 - \mu(D_0q_0) + \alpha q_0^3 + \beta q_0^2 + f\sin(\omega_0T_0 + \sigma T_1) + f\, q_0 \sin(\omega_0T_0 + \sigma T_1)$$

$$-p_1q_0 - d_1(D_0q_0) - \alpha_1q_0^3 - \alpha_2q_0^2(D_0q_0) - \alpha_3q_0(D_0q_0)^2 - G_1(D_0q_0)^3 \tag{3.5}$$

The solution of Eq (3.4) is:

$$q_0 = A(T_1)\mathrm{e}^{i\omega_0T_0} + cc. \tag{3.6}$$

where $A(T_1)$ is complex function in T_1, cc locate for the complex conjugate of the preceding terms.

Substitute Eq (3.6) for Eq (3.5), we get

$$\left(D_0^2+\omega_0^2\right)q_1=\begin{bmatrix}-2i\omega_0 D_1 A-i\mu\omega_0 A+3\alpha A^2\overline{A}-\dfrac{i}{2}f\,e^{i\sigma T_1}-p_1 A-id_1\omega_0 A-3\alpha_1 A^2\overline{A}\\ -3i\omega_0\alpha_2 A^2\overline{A}-\alpha_3\omega_0^2 A^2\overline{A}-i\omega_0^3 G_1 A^2\overline{A}\end{bmatrix}e^{i\omega_0 T_0}$$
$$+\left[\alpha A^3-\alpha_1 A^3-i\omega_0\alpha_2 A^3+\omega_0^2\alpha_3 A^3+i\omega_0^3 G_1 A^3\right]e^{3i\omega_0 T_0}+\beta A^2 e^{2i\omega_0 T_0}$$
$$+\beta\, A\overline{A}+\frac{f}{2}A\,e^{i(2\omega_0 T_0+\sigma T_1)}+\frac{f}{2}\overline{A}\,e^{i\sigma T_1}+cc \tag{3.7}$$

Removing the secular terms from Eq (3.7), we acquire

$$-2i\omega_0 D_1 A-i\mu\omega_0 A+3\alpha A^2\overline{A}-i\frac{f}{2}e^{i\sigma T_1}-p_1 A-id_1\omega_0 A-3\alpha_1 A^2\overline{A}-3i\omega_0\alpha_2 A^2\overline{A}$$
$$-\alpha_3\omega_0^2 A^2\overline{A}-i\omega_0^3 G_1 A^2\overline{A}=0 \tag{3.8}$$

Let $A=\frac{1}{2}a\,e^{i\delta}$ and substituting it into Eq (3.8) and separating the real and imaginary part yield the averaged equation as follows:

$$a'=-\frac{\mu}{2}a-\frac{f}{2\omega_0}\cos\theta-\frac{d_1}{2}a-\frac{3\alpha_2}{8}a^3-\frac{\omega_0^2 G_1}{8}a^3 \tag{3.9}$$

$$a\,\theta'=\sigma a-\frac{p_1}{2\omega_0}a+\frac{f}{2\omega_0}\sin\theta+\frac{3\alpha}{8\omega_0}a^3-\frac{3\alpha_1}{8\omega_0}a^3-\frac{\omega_0\alpha_3}{8}a^3 \tag{3.10}$$

where, $\theta=\sigma T_1-\delta$. The frequency response relations are then acquired as follows:

$$\sigma^2+\left\{\frac{-p_1}{\omega_0}+\frac{3\alpha}{4\omega_0}a^2-\frac{3\alpha_1}{4\omega_0}a^2-\frac{\omega_0\alpha_3}{4}a^2\right\}\sigma+$$
$$\left\{\begin{array}{l}\left[\dfrac{\mu^2}{4}+\dfrac{d_1^2}{4}+\dfrac{\mu d_1}{2}+\dfrac{p_1^2}{4\omega_0^2}-\dfrac{f^2}{4\omega_0^2a^2}\right]\\ +\left[\dfrac{3\mu\alpha_2}{8}+\dfrac{\mu\omega_0^2 G_1}{8}+\dfrac{3d_1\alpha_2}{8}+\dfrac{\omega_0^2 d_1 G_1}{8}-\dfrac{3\alpha p_1}{8\omega_0^2}+\dfrac{3\alpha_1 p_1}{8\omega_0^2}+\dfrac{\alpha_3 p_1}{8}\right]a^2+\\ \left[\dfrac{9\alpha_2^2}{64}+\dfrac{\omega_0^2 G_1^2}{64}+\dfrac{3\alpha_2\omega_0^2 G_1}{32}+\dfrac{9\alpha^2}{64\omega_0^2}+\dfrac{9\alpha_1^2}{64\omega_0^2}+\dfrac{\omega_0^2\alpha_3^2}{64}-\dfrac{9\alpha\alpha_1}{32\omega_0^2}-\dfrac{3\alpha\alpha_3}{32}+\dfrac{3\alpha_1\alpha_3}{32}\right]a^4\end{array}\right\} \tag{3.11}$$

Using the Newton-Raphson method and Matlab software, the steady-state responses may then be extracted from the algebraic equations. Using the Lyapunov first technique, the right-hand side eigenvalues of the Jacobian matrix at Eqs (3.9) and (3.10) are calculated, and the stability of the steady-state shell system is evaluated as follows:

$$\begin{bmatrix} a' \\ \theta' \end{bmatrix} = \begin{bmatrix} R_{11} & R_{12} \\ R_{21} & R_{22} \end{bmatrix} \begin{bmatrix} a \\ \theta \end{bmatrix} \tag{3.12}$$

where,

$$R_{11} = \frac{\partial a'}{\partial a} = -\frac{1}{2}(\mu + d_1) - (\frac{9\alpha_2}{8} + \frac{3\omega_0^2 G_1}{8})a^2, \qquad R_{12} = \frac{\partial a'}{\partial \theta} = \frac{f}{2\omega_0}\cos\theta,$$

$$R_{21} = \frac{\partial \theta'}{\partial a} = \frac{\sigma}{a} - \frac{p_1}{2\omega_0 a} + (\frac{9\alpha}{8\omega_0} - \frac{9\alpha_1}{8\omega_0} - \frac{3\omega_0\alpha_3}{8})a, \qquad R_{22} = \frac{\partial \theta'}{\partial \theta} = -\frac{f}{2\omega_0 a}\sin\theta$$

The previous matrix acquires the stable regions of the controlled model by solving the following determinant:

$$\begin{vmatrix} R_{11} - \lambda & R_{12} \\ R_{21} & R_{22} - \lambda \end{vmatrix} = 0 \tag{3.13}$$

Then,

$$\lambda^2 + \rho_1 \lambda^2 + \rho_2 = 0 \tag{3.14}$$

where, λ signifies the eigenvalue of the Jacobian matrix, $\rho_1 = -R_{11} - R_{22}$ and $\rho_2 = R_{11}R_{22} - R_{12}R_{21}$. The sufficient and necessary conditions for the structure to be stable according to Routh-Hurwitz criterion are $\rho_1 > 0$ and $\rho_2 > 0$. If the eigenvalues have negative real parts, the system is stable; otherwise, it is unstable. In frequency response curves, stable and unstable periodic responses are indicated by solid and dotted lines, respectively.

3.2. ½ Subharmonic resonance case $\omega_0 = \frac{1}{2}\omega$

We introduce the detuning parameter σ in accordance with Eq (2.7) analysis of subharmonic resonance as

$$\omega_0 = \frac{1}{2}\omega + \varepsilon\sigma \tag{3.15}$$

Substituting Eqs (3.6) and (3.5) into Eq (2.7) and equating coefficients of similar power of ε yields the following:

$O\left(\varepsilon^0\right)$:

$$\left(D_0^2+\frac{1}{4}\omega^2\right)q_0=0 \tag{3.16}$$

$O\left(\varepsilon^1\right)$:

$$\left(D_0^2+\frac{1}{4}\omega^2\right)q_1=-2(D_1D_0)q_0-\omega\sigma q_0-\mu(D_0q_0)+\alpha q_0^3+\beta q_0^2+f\sin(\omega T_0)+f\,q_0\sin(\omega T_0)$$

$$-p_1q_0-d_1(D_0q_0)-\alpha_1q_0^3-\alpha_2q_0^2(D_0q_0)-\alpha_3q_0(D_0q_0)^2-G_1(D_0q_0)^3 \tag{3.17}$$

The solution of Eq (3.16) is:

$$q_0=A(T_1)\,\mathrm{e}^{i\omega T_0/2}+cc. \tag{3.18}$$

where $A(T_1)$ is complex function in T_1, cc locate for the complex conjugate of the preceding terms. Substitute Eq (3.18) in Eq (3.17) yields:

$$\left(D_0^2+\frac{1}{4}\omega^2\right)q_1=\left[\begin{array}{l}-i\omega D_1A-\omega\sigma A-\frac{i}{2}\mu\omega A+3\alpha A^2\overline{A}-p_1A-\frac{i}{2}d_1\omega A\\ -3\alpha_1A^2\overline{A}-\frac{3}{2}i\omega\alpha_2A^2\overline{A}-\frac{1}{4}\alpha_3\omega^2A^2\overline{A}-\frac{3}{8}i\omega^3G_1A^2\overline{A}\end{array}\right]e^{i\omega T_0/2}$$

$$+\left[\alpha A^3-\alpha_1A^3-\frac{i}{2}\omega\alpha_2A^3-\frac{i}{2}fA+\frac{1}{4}\omega^2\alpha_3A^3+\frac{i}{8}\omega^3G_1A^3\right]e^{3i\omega T_0/2}$$

$$+\left[\beta A^2-\frac{i}{2}f\right]e^{i\omega T_0}+\beta A\overline{A}+cc \tag{3.19}$$

The secular terms of Eq (3.19) vanish if and only if

$$-i\omega D_1A-\omega\sigma A-\frac{i}{2}\mu\omega A+3\alpha A^2\overline{A}-p_1A-\frac{i}{2}d_1\omega A-3\alpha_1A^2\overline{A}$$
$$-\frac{3}{2}i\omega\alpha_2A^2\overline{A}-\frac{1}{4}\alpha_3\omega^2A^2\overline{A}-\frac{3}{8}i\omega^3G_1A^2\overline{A}=0 \tag{3.20}$$

Let $A=\frac{1}{2}a\,e^{i\gamma}$ and substituting it into Eq (3.20) and separating the real and imaginary parts yield the averaged equation as follows:

$$a'=-\frac{\mu}{2}a-\frac{d_1}{2}a-\frac{3\alpha_2}{8}a^3-\frac{3\omega^2G_1}{32}a^3 \tag{3.21}$$

$$a\gamma' = \sigma a + \frac{p_1}{\omega}a - \frac{3\alpha}{4\omega}a^3 + \frac{3\alpha_1}{4\omega}a^3 + \frac{\omega\alpha_3}{16}a^3 \tag{3.22}$$

For steady-state solutions, $a' = \gamma' = 0$ and the periodic solution at the fixed points corresponding to Eqs (3.21) and (3.22) is given by:

$$-\frac{\mu}{2}a - \frac{d_1}{2}a - \frac{3\alpha_2}{8}a^3 - \frac{3\omega^2 G_1}{32}a^3 = 0 \tag{3.23}$$

$$\sigma a + \frac{p_1}{\omega}a - \frac{3\alpha}{4\omega}a^3 + \frac{3\alpha_1}{4\omega}a^3 + \frac{\omega\alpha_3}{16}a^3 = 0 \tag{3.24}$$

As a result, the frequency response relationships are obtained as follows:

$$\sigma^2 + \left\{\frac{2p_1}{\omega} - \frac{3\alpha}{2\omega}a^2 + \frac{3\alpha_1}{2\omega}a^2 + \frac{\omega\alpha_3}{8}a^2\right\}\sigma + \left[\frac{\mu^2}{4} + \frac{d_1^2}{4} + \frac{\mu d_1}{2} + \frac{p_1^2}{\omega^2}\right]$$
$$+\left[\frac{3\mu\alpha_2}{8} + \frac{3\mu\omega^2 G_1}{32} + \frac{3d_1\alpha_2}{8} + \frac{3\omega^2 d_1 G_1}{32} - \frac{3\alpha p_1}{2\omega^2} + \frac{3\alpha_1 p_1}{2\omega^2} + \frac{\alpha_3 p_1}{8}\right]a^2 + \left[\frac{9\alpha_2^2}{64} + \frac{9\omega^2 G_1^2}{1024}\right.$$
$$\left.+\frac{9\alpha_2\omega^2 G_1}{128} + \frac{9\alpha^2}{16\omega^2} + \frac{9\alpha_1^2}{16\omega^2} + \frac{\omega^2\alpha_3^2}{256} - \frac{9\alpha\alpha_1}{8\omega^2} - \frac{3\alpha\alpha_3}{32} + \frac{3\alpha_1\alpha_3}{32}\right]a^4 = 0 \tag{3.25}$$

We offer the following forms to assess the stability of the fixed point solutions of Eqs (3.23) and (3.24).

$$A = ((p - iq)/2)e^{i\sigma T_1} \tag{3.26}$$

where p, q are real coefficients. Substitution of Eq (3.26) for the linearized form of Eq (3.20), we get:

$$-i\omega A' - \omega\sigma A - \frac{i}{2}\mu\omega A - p_1 A - \frac{i}{2}d_1\omega A = 0 \tag{3.27}$$

We get the following equations by substituting Eq (3.26) into Eq (3.27) and then equating the imaginary and real parts:

$$p' + (\frac{\mu}{2} + \frac{d_1}{2})p + (\frac{-p_1}{\omega})q = 0 \tag{3.28}$$

$$q' + (\frac{p_1}{\omega})p + (\frac{\mu}{2} + \frac{d_1}{2})q = 0 \tag{3.29}$$

The zeros of the characteristic equation determine the stability of a certain fixed point with regard to a proportional $\exp(\lambda T_1)$:

$$\begin{vmatrix} (\lambda+\frac{1}{2}(\mu+d_1)) & \frac{p_1}{\omega} \\ -\frac{p_1}{\omega} & (\lambda+\frac{1}{2}(\mu+d_1)) \end{vmatrix}=0 \tag{3.30}$$

where, λ is the eigenvalue. To analyze the stability of the non-trivial solution, one uses Eq (3.30) to obtain:

$$\lambda^2+r_1\lambda^2+r_2=0 \tag{3.31}$$

where, $r_1=(\mu+d_1)$ and $r_2=\frac{\mu^2}{4}+\frac{d_1^2}{4}+\frac{\mu d_1}{2}+\frac{p_1^2}{\omega^2}$ are constants. The Routh-Hurwitz criterion states that the following conditions must be met in order for all of Eq (3.31) roots to have negative real parts: $r_1 \succ 0,$ and $r_2 \succ 0$. If the eigenvalues have negative real parts, the system is stable; otherwise, it is unstable. Solid or dotted lines on frequency response curves denote stable or unstable periodic responses, respectively.

4. Numerical response influence outcomes

4.1. The new active vibration control influences at the primary resonance case $\omega \cong \omega_0$

Using the Runge-Kutta algorithm and the MATLAB 20.0 software, the original system Eqs (2.6) and (2.7) are numerically depicted in this section. Figure 2 displays the model's responses and phase-plane at primary resonance $\omega \cong \omega_0$ one of the worst resonance instances), and zero initial. Furthermore, Figure 3 illustrates the response and phase-plane for the nonlinear dynamical system with NNPDCVF in the primary resonance situation $\omega \cong \omega_0$, where the initial values $q(0)=0.5, \dot{q}(0)=0.5$ are used. The system's amplitude $q(t)$ is dramatically reduced, as seen in Figure 3. Additionally, using the NNPDCVF controller close to the primary resonance case that was measured, we will confirm all effects occurring in model parameters in this branch. As shown in Figures 2 and 3, the frequency response equations (FRE) defined by Eqs (3.9) and (3.10) were resolved and plotted by matching parameter values. Figure 4 shows the response diagram for the controlled system a against the detuning value σ. Stable solutions are represented by solid lines presented graphically by (———), whereas unstable solutions refer by dashed lines presented graphically by (-----). In this figure stable areas are less than the unstable regions. The steady state amplitude a is monotonic decreasing function of the linear damping coefficient μ and monotonic increasing function of the natural angular frequency coefficient ω_0 showing the stable and unstable regions as plotted in Figure 5a,b, respectively. Figure 6a presents when the nonlinear parameter α decrease the curve is bent slightly to the right making increasing in instability zones, while the nonlinear control parameter α_1 decrease the curve is bent to the left making increasing in stability zones illustrated in Figure 6b, which gives an excellent result for controlling the model. Besides, when the nonlinear parameter α_2 decrease the amplitude a is decreased making decreasing in instability zones as plotted in Figure 7a, while the nonlinear control parameter α_3 decrease the curve is bent to the left making increasing in stability zones demonstrated in Figure 7b, which gives excellent result for

controlling the model. Moreover, the steady-state amplitude a is increased with increasing the excitation coefficient f making increasing in the unstable area as exemplified in Figure 8a, while at choosing lessen values of p_1 the amplitude a is bent slightly to right making increasing the area of stable regions as plotted in Figure 8b. Furthermore, Figure 9a presents that when the values of the linear control force parameter d_1 decreased the amplitude a is increased appearing the stable and unstable regions, whereas, at lessen values of the gain coefficient G_1 the amplitude a is increased with increasing in instability counties as seen in Figure 9b.

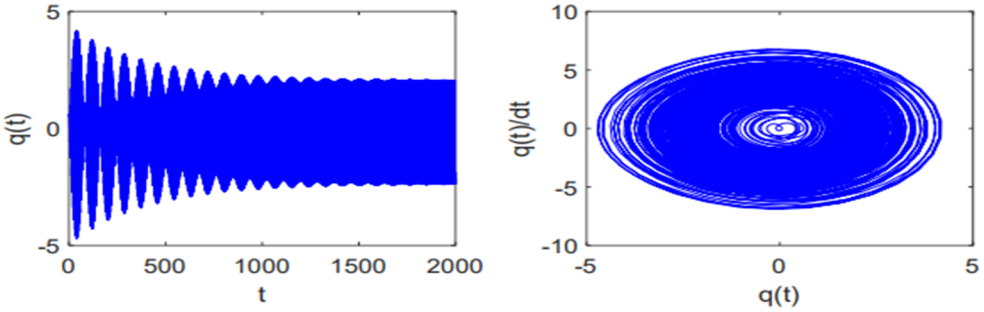

Figure 2. Response of the framework without controller on primary resonance.

$(\mu = 0.02; \omega = 1.5; \alpha = 0.15; \beta = 0.02; f = 2.15; \omega \cong \omega_0)$.

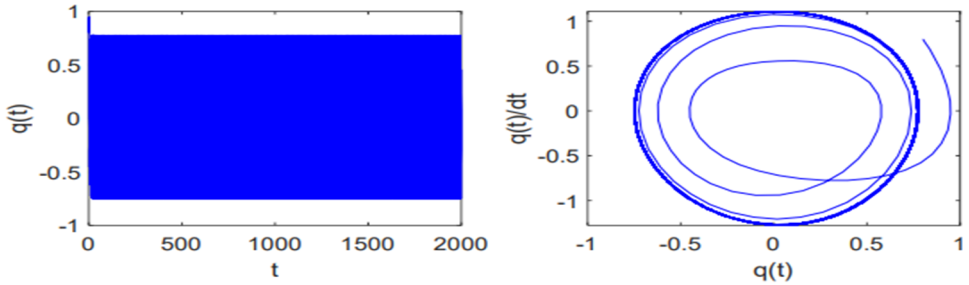

Figure 3. Response of the model with NNPDCVF controller on primary resonance case.

$(\mu = 0.02, \omega = 1.5, \alpha = 0.15, \beta = 0.02, f = 2.15, \omega \cong \omega_0, p_1 = 0.5, d_1 = 1.2, \alpha_1 = 0.3, \alpha_2 = 0.4, \alpha_3 = 0.25, G_1 = 0.5)$.

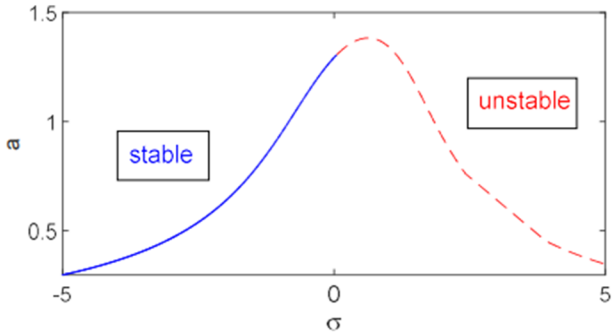

Figure 4. Frequency-response diagram over the controlled model within primary resonance case $\omega \cong \omega_0$.

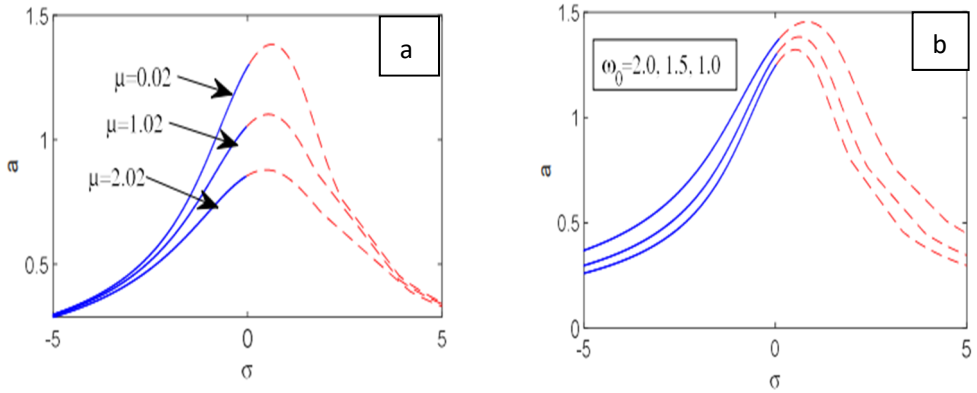

Figure 5. Effect outcomes of (a) damping coefficient μ and (b) the natural angular frequency ω_0.

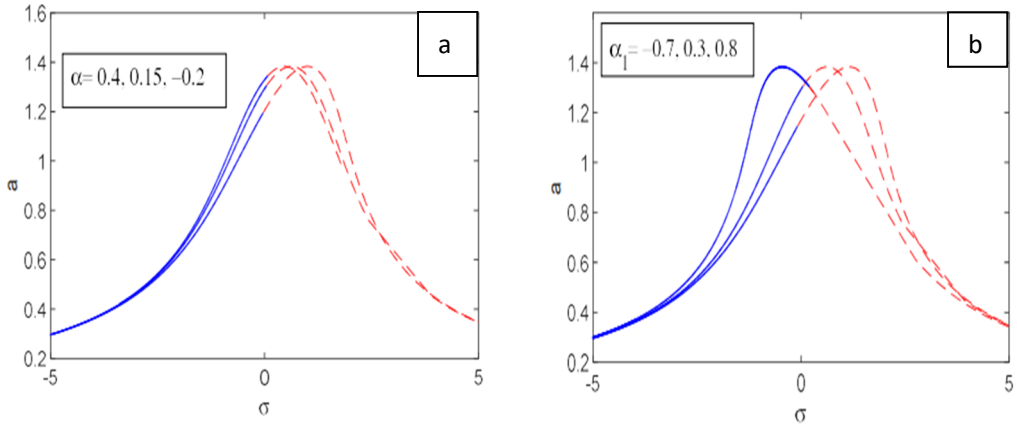

Figure 6. Effect outcomes of (a) nonlinear coefficient α and (b) the nonlinear control parameter α_1.

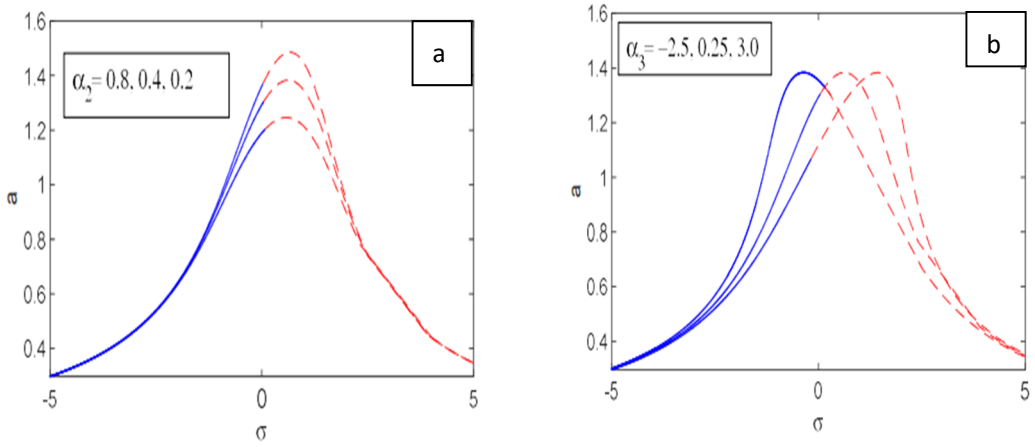

Figure 7. Effect outcomes of (a) nonlinear control coefficient α_2 and (b) the nonlinear control parameter α_3.

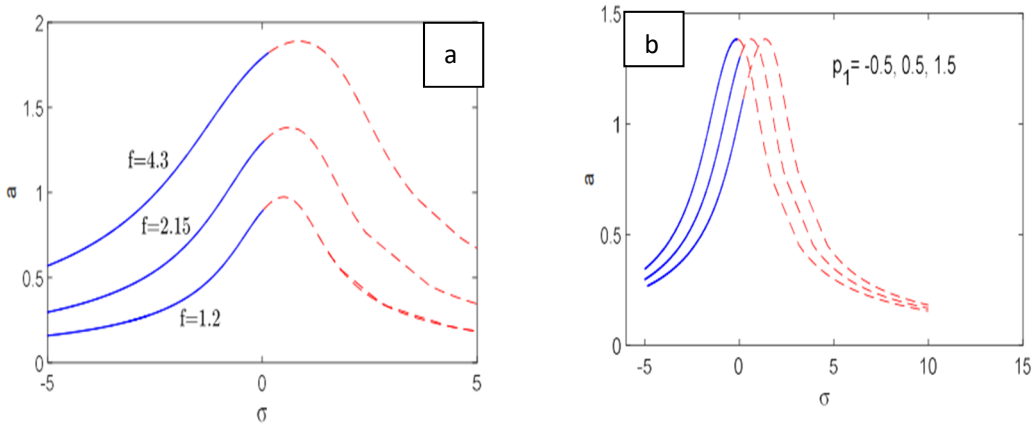

Figure 8. Effect outcomes of (a) excitation force f and (b) the linear control force p_1.

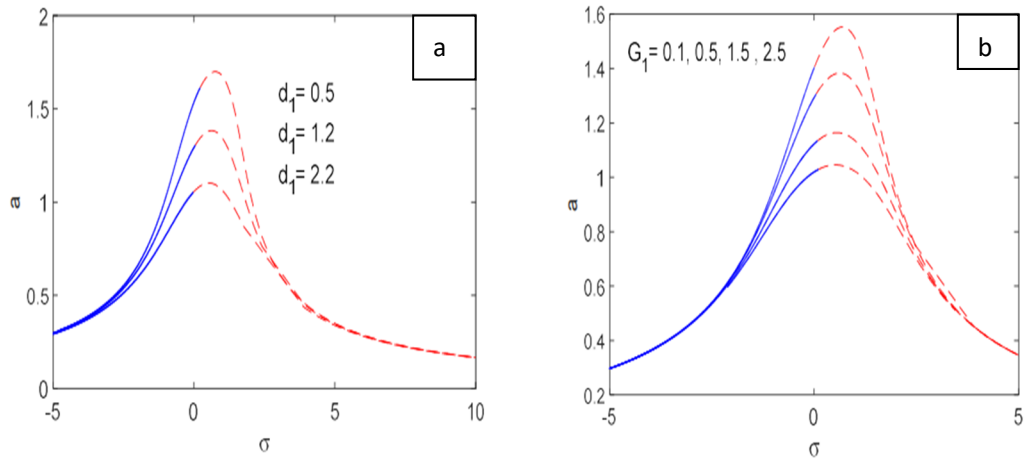

Figure 9. Effect outcomes of (a) the linear control force d_1 and (b) the gain coefficient G_1.

4.2. The new active vibration control impacts at ½ Subharmonic resonance $\omega_0 = \omega/2$

In this section, Figure 10 shows responses and phase-plane of the framework with no controller on the ½ subharmonic resonance $\omega_0 = \omega/2$ (one of worse resonance cases) within zero initial. Also, Figure 11 conclude the response and phase-plane for the nonlinear dynamical framework with NNPDCVF on $\omega_0 = \omega/2$ with the initial values $q(0) = 0.5, \dot{q}(0) = 0.5$. The amplitudes of the system $q(t)$ is decreased dramatically as appeared in Figure 11. Additionally, we will verify all model parameter changes with the NNPDCVF controller in this branch, which is close to the measured subharmonic resonance condition. As shown in Figures 10 and 11, the frequency response equations (FRE) given by Eqs (3.21) and (3.22) were resolved and plotted by matching parameter values. Figure 12 displays the response diagram aimed at the controlled framework a versus detuning coefficient σ. Only stable solutions is appeared which stand by solid lines presented graphically by (———), without any unstable solutions. This refers to that the new active controller made the system more stable in this resonance case. The steady state amplitude value a is decreasing when the linear damping coefficient μ values are decreased as designed in Figure 13. Also, Figure 14 presents the effect outcomes of the natural angular frequency ω as when it increased the steady-state amplitude a is also increased. Moreover, when the values of the nonlinear coefficient α are decreased the values of the amplitude a are lessen as seen in Figure 15. On the other hand, Figure 16 shows that when the values of the nonlinear control coefficient α_1 are decreased the values of the amplitude a are increased. Besides, the amplitude a is increased when the values of the nonlinear control parameter α_2 are increased as strategized in Figure 17. Furthermore, the values of the nonlinear control parameter α_3 are increased when the values of a are decreased as shown in Figure 18. Additionally, Figure 19 appears a special effect of the linear control force p_1 as when it takes an increasing values, the curve is shifted to the right without any change influence in the amplitude behavior diagram. In addition, at increasing values of the linear control force d_1, value of a is decreased as realized in Figure 20. Finally, at lessen values of the gain coefficient G_1 the value of a is increased with increasing in stability regions as seen in Figure 21.

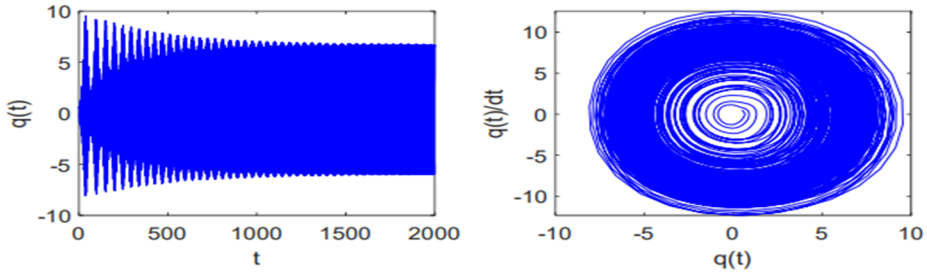

Figure 10. Response of the system with no controller at sub-harmonic resonance case $\omega_0 \cong \omega/2$.

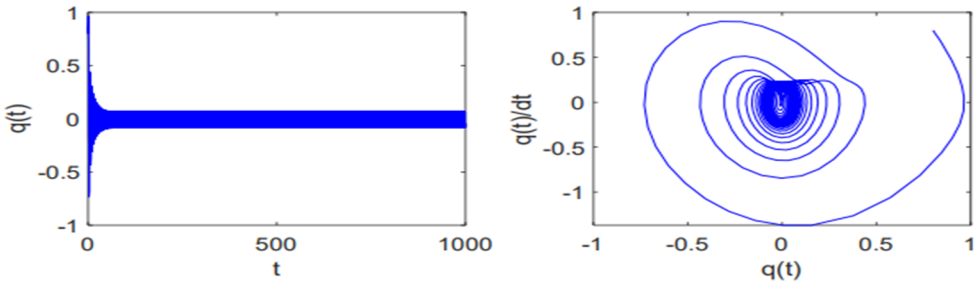

Figure 11. Response of the system with NNPDCVF controller at sub-harmonic resonance case $\omega_0 \cong \omega/2$.

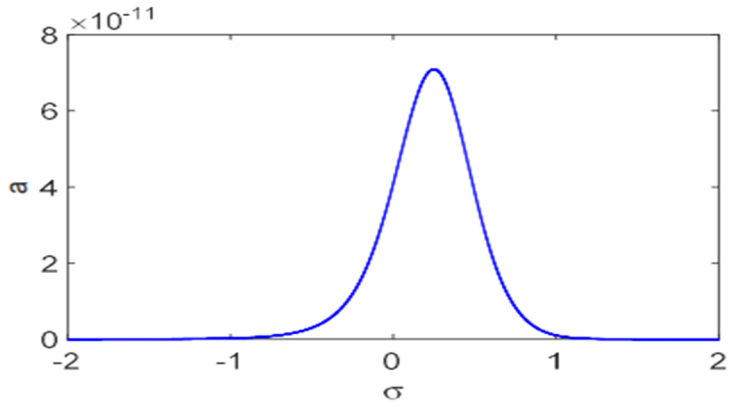

Figure 12. Frequency-response chart on the controller system at sub-harmonic resonance case $\omega_0 \cong \omega/2$ within the values $(\mu = 0.2, \omega = 1.5, \alpha = 0.5,\ p_1 = 0.5, d_1 = 1.2, \alpha_1 = 0.3, \alpha_2 = 0.4, \alpha_3 = 0.5, \mathrm{G}_1 = 0.5)$.

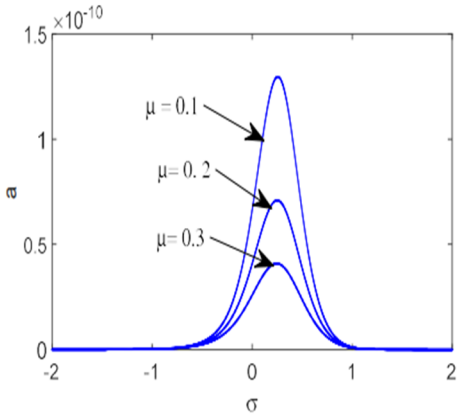

Figure 13. Influence diagram of the damping coefficient μ.

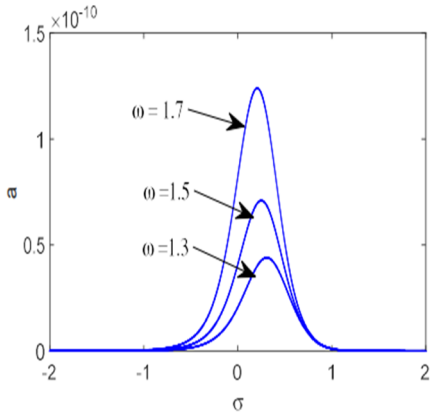

Figure 14. Influence diagram of the natural angular frequency ω.

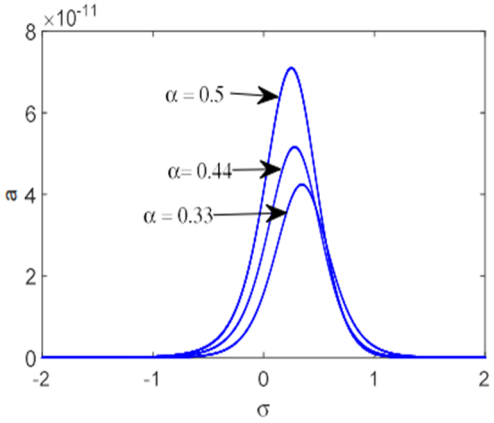

Figure 15. Influence diagram of nonlinear coefficient α.

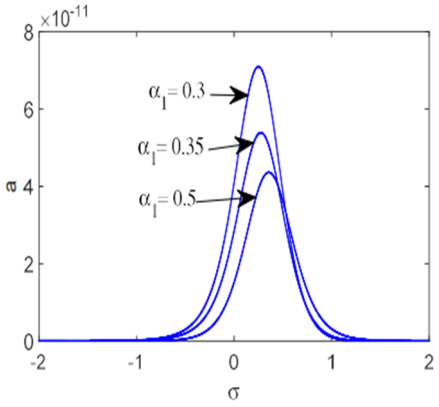

Figure 16. Influence graph of the nonlinear control the parameter α_1.

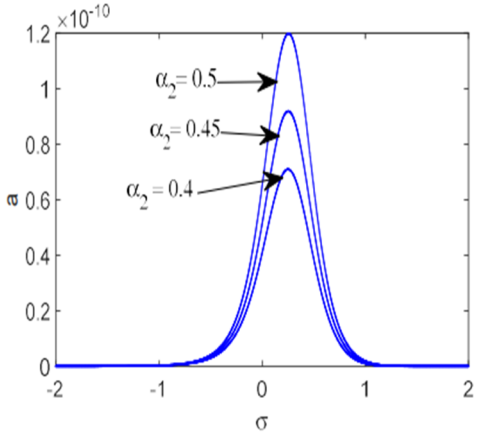

Figure 17. Influence curve of the nonlinear control parameter α_2.

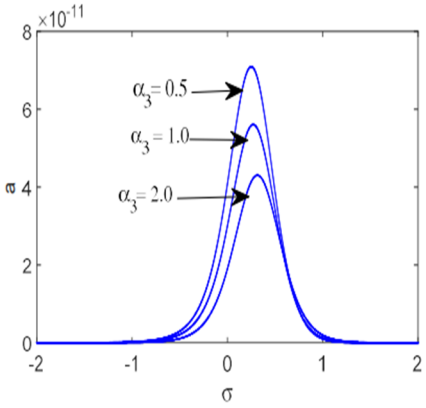

Figure 18. Influence chart of the nonlinear control parameter α_3.

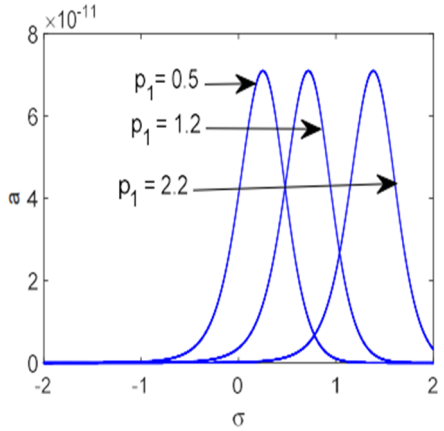

Figure 19. Influence diagram of the linear control force p_1.

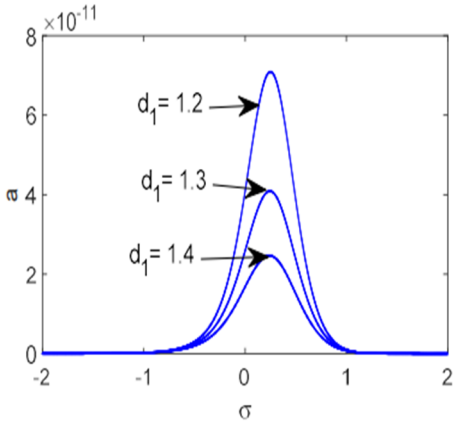

Figure 20. Influence diagram of the linear control force d_1.

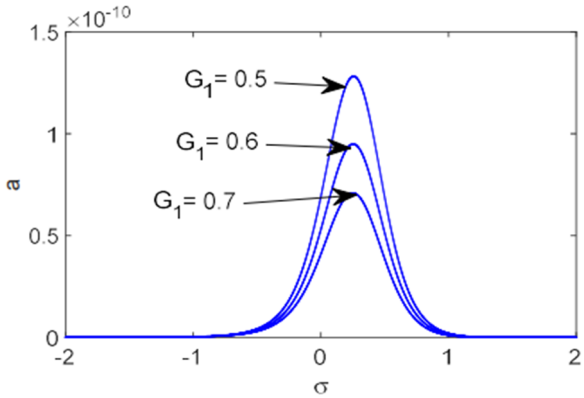

Figure 21. Influence diagram of the gain coefficient G_1.

5. The optimum control parameters

The mechanism of the NNPDCVF controller at the primary resonance can be explained simply with the aid of Eqs (3.9) and (3.10). It is clear from Eqs (3.9) and (3.10) that the integration of the NNPDCVF controller to the considered system has modified the linear damping term μ to the controlled term $\mu_{primary}$. Moreover, the detuning parameter σ is modified to $\sigma_{primary}$, where $\mu_{primary}$ and $\sigma_{primary}$ are given as follows:

$$\mu_{primary} = \frac{1}{2}(\mu + d_1) \tag{5.1}$$

$$\sigma_{primary} = \sigma - \frac{p_1}{2\omega_0} \tag{5.2}$$

It is clear from Eqs (5.1) and (5.2) that $\mu_{primary}$ and $\sigma_{primary}$ are periodic functions on the controller, where the controlled system has the equivalent linear damping $\mu_{primary} = \frac{1}{2}(\mu + d_1)$ and detuning parameter $\sigma_{primary} = \sigma - \frac{p_1}{2\omega_0} = \omega - (\omega_0 + \frac{p_1}{2\omega_0})$. This means that the linear control force (p_1) is responsible for changing the system natural frequency (ω_0), while the velocity gain (d_1) is responsible for modifying the system linear damping coefficient (μ). Accordingly, to improve the vibration suppression efficiency of the considered system, the linear control forces (p_1, d_1) should be selected in a way that maximizes the objective function $\mu_{primary}$ and $\sigma_{primary}$. By comparing the obtained results in Figures 8(b) and 9(a) with the objective function given by Eqs (5.1) and (5.2), we can notice that the best vibration suppression condition has occurred at the maximum values of $\mu_{primary}$ and $\sigma_{primary}$ as summarized in Table 1. It is worth to mention that the same mechanism occurred at the ½ subharmonic resonance cases. The objective functions in the ½ subharmonic resonance can be deduced simply from Eqs (3.21) and (3.22), respectively, where $\mu_{sub} = \frac{1}{2}(\mu + d_1)$, $\sigma_{sub} = \sigma + \frac{p_1}{\omega}$.

Table 1. Optimum control parameter.

Figure	p_1	d_1	ω_0	$\mu_{primary} = \frac{1}{2}(\mu + d_1)$	$\sigma_{primary} = \sigma - \frac{p_1}{2\omega_0}$	Max ($\mu_{primary}$)	Max($\sigma_{primary}$)
Figure 8b	-0.5	0.0	1.5	$\frac{1}{2}(\mu + 0)$	$\sigma + \frac{0.5}{2(1.5)}$	0.5μ	$\sigma + \frac{1}{6}$
Figure 9a	0.0	2.2	1.5	$\frac{1}{2}(\mu + 2.2)$	$\sigma + 0$	$0.5\mu + 1.1$	σ

6. Verification of analytical solutions using numerical simulation solutions

The system which set by Eq (2.7) solved numerically at the two resonances which are primary case where ($\omega \cong \omega_0$) and ½ subharmonic resonance cases where ($\omega_0 \cong \omega / 2$) compared with the analytical solution of the modulating Eqs (3.8) and (3.20), respectively as presented in Figure 22. On

the other hand, the continuous lines symbolize the time histories which obtained numerically (using Runge-Kutta method) for Eq (2.7) and the dashed lines confirm inflection of amplitude for the coordinate $q(t)$ at similar values of parameters which using in Figure 3.

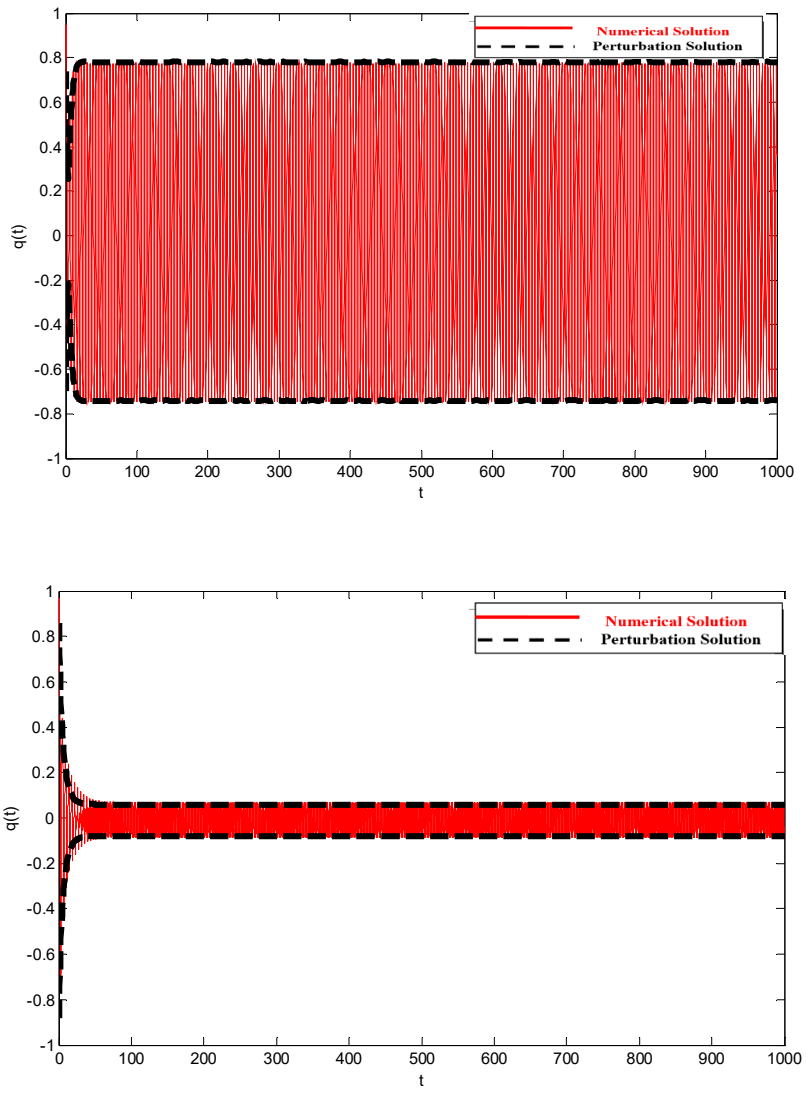

Figure 22. Relationship connecting numerical solution (using Runge-kutta method) and mathematical solution (using perturbation method) of the system and NNPDCVF.

7. Conclusions

A novel control technique is used to investigate the response of a moving load excited nonlinear dynamic system to nonlinear primary resonances and 1/2 subharmonic resonances. The controller NNPDCVF reduces the vibration amplitude of the two resonances. The stability analysis via NNPDCVF on the two measured resonances is studied and investigated using MATLAB software. The effect of various effective control system parameters on the outcome is discussed. In the case of primary resonance, a suitable choice of some effective coefficients can reduce the response's peak

amplitude (or the free oscillation term's peak amplitude) and the unstable regions. Using the new controller, the instability solutions for 1/2 subharmonic resonance are minimized in this case. Only stable solutions were found, indicating that in this situation the new controller is the best. Optimal control parameters are calculated. Finally, numerical confirmations for all obtained analytical results are introduced

Acknowledgments

The author would like to thank an editor and an anonymous reviewer whose insightful comments have helped to improve the quality of this paper considerably.

Conflict of interests

The authors declare that there is no conflict of interest.

References

1. P. Avitable, Twenty years of structural dynamic modification-a review, *Sound Vib.*, **37** (2003), 14–27.
2. M. Nad, Modification of modal characteristics of vibrating structural elements, *Scientific Monographs, Köthen*, 2010.
3. M. Sága, M. Žmindák, V. Dekýš, A. Sapietová, Š. Segľa, Selected methods for the analysis and synthesis of mechanical systems, *VTS ZU, Zilina*, (2009).
4. D. St˘ancioiu, H. Ouyang, J. E. Mottershead, Vibration of a beam excited by a moving oscillator considering separation and reattachment, *J. Sound Vib*., **310** (2008), 1128–1140. https://doi.org/10.1016/j.jsv.2007.08.019
5. L. Sun, Dynamic displacement response of beam-type structures to moving line loads, *Int. J. Solids Struct*., **38** (2001), 8869–8878. https://doi.org/10.1016/s0020-7683(01)00044-0
6. S. Y. Lee, S. S. Yhim, Dynamic analysis of composite plates subjected to multi-moving loads based on a third order theory, *Int. J. Solids Struct.*, **41** (2004), 4457–4472. https://doi.org/10.1016/j.ijsolstr.2004.03.021
7. A.V. Pesterev, L. A. Bergman, A contribution to the moving mass problem, *J. Vib. Acoust.*, **120** (1998), 824–826. https://doi.org/10.1115/1.2893904
8. N. Azizi, M. M. Saadatpour, M. Mahzoon, Using spectral element method for analyzing continuous beams and bridges subjected to a moving load, *Appl. Math. Model.*, **36** (2012), 3580–3592. https://doi.org/10.1016/j.apm.2011.10.019
9. M. Dehestani, M. Mofid, A. Vafai, Investigation of critical influential speed for moving mass problems on beams, *Appl. Math. Model.*, **33** (2009), 3885–3895. https://doi.org/10.1016/j.apm.2009.01.003
10. A. Nikkhoo, F. R. Rofooei, M. R. Shadnam, Dynamic behavior and modal control of beams under moving mass, *J. Sound Vib.*, **306** (2007), 712–724. https://doi.org/10.1016/j.jsv.2007.06.008
11. S. Marchesiello, A. Fasana, L. Garibaldi, B. A. D. Piombo, Dynamics of multi-span continuous straight bridges subject to multi-degrees of freedom moving vehicle excitation, *J. Sound Vib*., **224** (1999), 541–561. https://doi.org/10.1006/jsvi.1999.2197

12. L. Fryba, *Vibration of Solids and Structures Under Moving Loads*, Thomas Telford, 1999. https://doi.org/10.1680/vosasuml.35393.0027
13. Z. C. Qiu, X. M. Zhang, H. X. Wu, H. H. Zhang, Optimal placement and active vibration control for piezoelectric smart flexible cantilever plate, *J. Sound Vib.*, **301** (2007), 521–543. https://doi.org/10.1016/j.jsv.2006.10.018
14. J. J. Liao, A. P. Wang, C. M. Ho, Y. D. Hwang, A robust control of a dynamic beam structure with time delay effect, *J. Sound Vib.*, **252** (2002), 835–847. https://doi.org/10.1006/jsvi.2001.3772
15. C. M. Casado, I. M. Díaz, J. Sebastián, A. V. Poncela, A. Lorenzana, Implementation of passive and active vibration control on an in-service footbridge, *Struct. Control Health Monit.*, **20** (2013), 70–87. https://doi.org/10.1002/stc.471
16. D. Younesian, E. Esmailzadeh, R. Sedaghati, Passive vibration control of beams subjected to random excitations with peaked PSD, *J. Vib. Control*, **12** (2006), 941–953. https://doi.org/10.1177/1077546306068060
17. R. Alkhatib, M. Golnaraghi, Active structural vibration control: a review, *Shock Vib.*, **35** (2003), 367–383. https://doi.org/10.1177/05831024030355002
18. S. Korkmaz, A review of active structural control: challenges for engineering informatics, *Comput. Struct.*, **89** (2011), 2113–2132. https://doi.org/10.1016/j.compstruc.2011.07.010
19. A. Nikkhoo, Investigating the behavior of smart thin beams with piezoelectric actuators under dynamic loads, *Mech. Syst. Signal. Process.*, **45** (2014), 513–530. https://doi.org/10.1016/j.ymssp.2013.11.003
20. I. D. Landau, A. Constantinescu, D. Rey, Adaptive narrow band disturbance rejection applied to an active suspension—an internal model principle approach, *Automatica*, **41** (2005), 563–574. https://doi.org/10.1016/j.automatica.2004.08.022
21. J. Liu, W. L. Qu, Y. L. Pi, Active/robust control of longitudinal vibration response of floating-type cable-stayed bridge induced by train braking and vertical moving loads, *J. Vib. Control*, **16** (2010), 801–825. https://doi.org/10.1177/1077546309106527
22. B. Xu, Z. Wu, K. Yokoyama, Neural networks for decentralized control of cable-stayed bridge, *J. Bridge Eng.*, **8** (2003), 229–236. https://doi.org/10.1061/(asce)1084-0702(2003)8:4(229)
23. K. C. Chuang, C. C. Ma, R. H. Wu, Active suppression of a beam under a moving mass using a pointwise fiber Bragg grating displacement sensing system, *IEEE Trans. Ultrason. Ferroelectr. Freq. Control*, **59** (2012), 2137–2148. https://doi.org/10.1109/tuffc.2012.2440
24. M. H. Ghayesh, H. A. Kafiabad, T. Reid, Sub- and super-critical nonlinear dynamics of a harmonically excited axially moving beam, *Int. J. Solids Struct.*, **49** (2012), 227–243. https://doi.org/10.1016/j.ijsolstr.2011.10.007
25. A. K. Mallik, S. Chandra, A. B. Singh, Steady-state response of an elastically supported infinite beam to a moving load, *J. Sound Vib.*, **291** (2006), 1148–1169. https://doi.org/10.1016/j.jsv.2005.07.031
26. S. Zheng, J. Lian, H. Wang, Genetic algorithm based wireless vibration control of multiple modal for a beam by using photostrictive actuators, *Appl. Math. Modell.*, **38** (2014), 437–450. https://doi.org/10.1016/j.apm.2013.06.032
27. D. J. Inman, *Vibration with Control*, John Wiley & Sons, Ltd., 2006. https://doi.org/10.1002/0470010533
28. T. Soong, *Active Structural Control: Theory and Practice*, Harlow, Longman Scientific & Technical, 1990.

29. M. I. Friswell, D. J. Inman, The relationship between positive position feedback and output feedback controllers, *Smart Mater. Struct.*, **8** (1999), 285–291. https://doi.org/10.1088/0964-1726/8/3/301
30. J. L. Fanson, T. K. Caughey, Positive position feedback control for large space structures, *AIAA J.*, **28** (1990), 717–724. https://doi.org/10.2514/3.10451
31. Y. G. Sung, Modelling and control with piezoactuators for a simply supported beam under a moving mass, *J. Sound Vib.*, **250** (2002), 617–626. https://doi.org/10.1006/jsvi.2001.3941
32. D. Stancioiu, H. Ouyang, Optimal vibration control of beams subjected to a mass moving at constant speed, *J. Vib. Control*, **22** (2016), 3202–3217. https://doi.org/10.1177/1077546314561814
33. J. Yang, J. Wu, A. Agrawal, Sliding mode control for nonlinear and hysteretic structures, *J. Eng. Mech.*, **121** (1995), 1330–1339. https://doi.org/10.1061/(asce)0733-9399(1995)121:12(1330)
34. K. D. Young, V. I. Utkin, U. Ozguner, A control engineer's guide to sliding mode control, *IEEE Trans. Control Syst. Technol.*, **7** (1999), 328–342. https://doi.org/10.1109/87.761053
35. Y. Pi, X. Wang, Trajectory tracking control of a 6-DOF hydraulic parallel robot manipulator with uncertain load disturbances, *Control Eng. Pract*., **19** (2011), 185–193. https://doi.org/10.1016/j.conengprac.2010.11.006
36. Z. C. Qiu, H. X. Wu, D. Zhang, Experimental researches on sliding mode active vibration control of flexible piezoelectric cantilever plate integrated gyroscope, *Thin Wall. Struct.*, **47** (2009), 836–846. https://doi.org/10.1016/j.tws.2009.03.003
37. H. S. Bauomy, A. T. El-Sayed, A new six-degrees of freedom model designed for a composite plate through PPF controllers, *Appl. Math. Modell.*, **88** (2020), 604–630. https://doi.org/10.1016/j.apm.2020.06.067
38. H. S. Bauomy, A. T. El-Sayed, Act of nonlinear proportional derivative controller for MFC laminated shell, *Phys. Scr.*, **95** (2020), 095210. https://doi.org/10.1088/1402-4896/abaa7c
39. H. S. Bauomy, A. T. El-Sayed, Mixed controller (IRC+NSC) involved in the harmonic vibration response cantilever beam model, *Meas. Control*, **53** (2020), 1954–1967. https://doi.org/10.1177/0020294020964243
40. A. T. El-Sayed, H. S. Bauomy, Outcome of special vibration controller techniques linked to a cracked beam, *Appl. Math. Modell.* **63** (2018), 266–287. https://doi.org/10.1016/j.apm.2018.06.045
41. H. S. Bauomy, New controller (NPDCVF) outcome of FG cylindrical shell structure, *Alexandria Eng. J.*, **61** (2022), 1779–1801. https://doi.org/10.1016/j.aej.2021.06.061
42. Y. Tang, T. Wang, Z. S. Ma, T. Yang, Magneto-electro-elastic modelling and nonlinear vibration analysis of bi-directional functionally graded beams, *Nonlinear Dyn.*, **105** (2021), 2195–2227. https://doi.org/10.1007/s11071-021-06656-0
43. Y. Tang, G. Wang, T. Ren, Q. Ding, T. Yang, Nonlinear mechanics of a slender beam composited by three-directional functionally graded materials, *Comp. Structs.*, **270** (2021), 114088. https://doi.org/10.1016/j.compstruct.2021.114088
44. Y. Tang, Z. S. Ma, Q. Ding, T. Wang, Dynamic interaction between bi-directional functionally graded materials and magneto-electro-elastic fields: A nano-structure analysis, *Comp. Structs.*, **264** (2021), 113746. https://doi.org/10.1016/j.compstruct.2021.113746

45. N. Navadeha, P. Sarehb, V. Basovskyc, I. Gorbanc, A. S. Fallah, Nonlinear vibrations in homogeneous non-prismatic Timoshenko cantilevers, *J. Comput. Nonlinear Dyn*., **16** (2021), 01002. https://doi.org/10.1115/1.4051820
46. C. Xie, Y. Wu, Z. Liu, Modeling and active vibration control of lattice grid beam with piezoelectric fiber composite using fractional order PD$^{\mu}$ algorithm, *Comp. Structs*., **198** (2018), 126–134. https://doi.org/10.1016/j.compstruct.2018.05.060
47. M. Azizi, S. Talatahari, P. Sareh, Design optimization of fuzzy controllers in building structures using the crystal structure algorithm (CryStAl), *Adv. Eng. Inf.*, **52** (2022), 101616. https://doi.org/10.1016/j.aei.2022.101616
48. M. Radgolchin, H. Moeenfard, An analytical approach for modeling nonlinear vibration of doubly clamped functionally graded Timoshenko microbeams using strain gradient theory, *Int. J. Dyn. Control*, **6** (2018), 990–1007. https://doi.org/10.1007/s40435-017-0369-8
49. A. H. Nayfeh, *Problems in Perturbation*, Wiley, New York, 1985.
50. A. H. Nayfe, D. T. Mook, *Nonlinear Oscillations*, Wiley, New York, 1995. https://doi.org/10.1002/9783527617586

AIMS Press